Topological Analysis of Multiple Metal−Metal Bonds in Dimers of the M_2(Formamidinate)$_4$ Type with M = Nb, Mo, Tc, Ru, Rh, and Pd

R. Llusar,*,† A. Beltrán,† J. Andrés,† F. Fuster,‡ and B. Silvi‡

Departament de Ciències Experimentals, Universitat Jaume I, Box 224, 12080 Castelló, Spain, and Laboratoire de Chimie Théorique, Université Pierre et Marie Curie, UMR-CNRS 7616, Paris, France

Received: May 17, 2001; In Final Form: July 30, 2001

The chemical bond in complexes of the M_2(formamidinate)$_4$ type with different nominal bond orders has been investigated within the framework of the present topological theories. The atoms-in-molecules (AIM) analysis of the theoretically calculated electron density shows low $\rho(r)$ values at the metal−metal bond critical point (r_c), which makes difficult a topological description of the interaction using the electron density as the scalar function. When the electron localization function (ELF) is used instead, four disynaptic metal−metal valence basins, V(M,M), are found for the Mo and Nb dimers, one for each the Ru and Rh complexes, while no disynaptic basins are obtained for the Tc and Pd systems. The V(M,M) basins are not the dominant features of the interaction due to their low population values with the main contribution arising from the "4d" metal electrons. However, the molecular orbitals involving the "4d" function of the metal essentially contribute to the metal core basins, C(M). The most important characteristic of the metal−metal bond is the abnormally high values for the metal−metal core covariance, B(M,M), and the AIM atomic basins covariances, $\lambda_c(\rho)$. This large electron fluctuation which occurs between the two metallic cores is interpreted in terms of simple resonance arguments. Except for Rh, there is an excellent correlation between the core covariances, B(M,M), and the metal−metal distances.

Introduction

Transition metal molecular compounds which offer the possibility of metal−metal bonds have been the subject of many experimental as well as theoretical investigations in the past 30 years.[1,2] Deeper knowledge on the electronic structure and bonding between two metal atoms is crucial for understanding metal−metal interactions. The reactivity and physical properties (metal−metal bond distances, paramagnetism and diamagnetism, electronic transitions, ionizations, and redox activity) of metal dimers can be qualitatively rationalized in terms of the general quadruple bond order scheme which formulates interactions between transition metal atoms in terms of overlaps of the metal "d" orbitals, giving rise to σ, π, and δ bonding and antibonding orbitals.[3] Whenever the number of electrons occupying the bonding orbitals exceeds those in the antibonding orbitals, metal−metal bonds will be formed, although ambiguity sometimes arise as to the bond order.

Detailed features of the above bonding scheme have mainly been studied in molecules of general formula M_2L_4 and an approximate D_{4h} symmetry for the ligand environment around the dimetal core. The structural properties of these second row metal dimers with a high structural symmetry can be quantitatively predicted using advanced quantum mechanical methodologies.[4−6] Specifically, Cotton and Feng have shown that accurate geometry optimizations using DFT methods can be carried out for tetrabridged compounds with a paddlewheel structure and a closed-shell electronic ground-state such as the formamidinate derivatives M_2(HNCHNH)$_4$ represented in Figure 1.[4] The

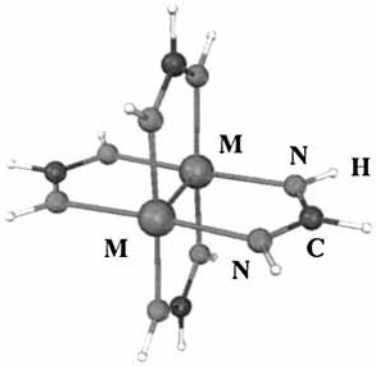

Figure 1. Ball and sticks representation of M_2(HNCHNH)$_4$.

success in this area is an indication of the reliability in the calculated electron density even for systems such as the Rh and Ru complexes for which the "nominal bond orders" assigned are in apparent contradiction with the experimental and calculated metal−metal distances. In addition, good estimates of the ionization energies based on several different density functionals have been obtained for these formamidinate complexes when M = Cr, Mo, and W.[7]

In the past years, topological formulations of the chemical bond have emerged which have provided a better understanding of its nature. Topological analyses of the metal−metal interactions raise the question whether bonds between transition metals may be treated in the same fashion as bonds between main group elements.[8,9] In Bader's analysis of the electron density, a shared interaction (i.e., a covalent bond) is characterized by a rather large value of the charge density, $\rho(r_c)$, at the bond critical point and by a negative value of the laplacian $\nabla^2\rho(r_c)$.[10] On the other hand, a closed-shell interaction presents a

* Corresponding author.
† Universitat Jaume I.
‡ Université Pierre et Marie Curie.

10.1021/jp011906+ CCC: $20.00
Published on Web 09/15/2001

low $\rho(r_c)$ value at the bond critical point and positive values of the Laplacian. These complementary criteria are related to the same physical idea, namely, that in a covalent bond there is concentration of electron density in the internuclear region.

It has been shown that complexes with a M−M interaction have small $\rho(r_c)$ values at the bond critical point and in general for these systems the closed-shell versus the open-shell classification based on the sign of the laplacian $\nabla^2\rho(r_c)$ is ambiguous.[9,11,12] It is worth noting that this situation is somewhat similar to that of F_2. In the last case energetic considerations derived from the application of the virial theorem to the critical point, together with a topological analysis of the Becke and Edgecombe localization function (ELF), enable one to unambiguously characterize the F−F bond as covalent.[13,14]

The purpose of this work is to examine topologically the metal−metal interactions in some metallic dimers of formula $M_2(HNCHNH)_4$ (M = Nb, Mo, Tc, Ru, Rh, and Pd) for which experimental structural data are available, with the exception of Nb and Tc, and accurate electron densities have been calculated for their singlet ground states using DFT methods. All these model systems are neutral, and therefore, the problem of counterion interaction is eliminated. These various complexes provide a series of isostructural compounds differing only in the nature of the metal and consequently in the number of electrons available for the metal−metal bond. The nominal bond order estimated on the basis of the quadruple bonded molecular orbital scheme is four for Mo, three for Nb and Tc, two for Ru, one for Rh, and zero for Pd.

The paper is organized as follows: the first section provides a survey of the topological analysis of the electron localization function (ELF). Then the possibilities of the ELF method are exemplified on the $Mo_2(HNCHNH)_4$ molecule, for which a detailed analysis is presented along with a critical comparison with "atoms-in-molecules" (AIM) based techniques. The bonding in the remaining tetraformamidinate complexes and the evolution with respect to the nature of the transition metal are discussed in the last section before the conclusion.

2. Topological Analysis of the Electron Localization Function

Chemical concepts are defined within the framework of present topological theories in terms of the mathematical properties of the gradient vector field of a given local function, $f(r)$, called the potential function. This analysis enables the partitioning of the space into well-defined regions, basins, bounded by separatrices. The chemical meaning of a basin is the cornerstone of this approach, and obviously, it depends on the nature of the function $f(r)$. In the case of the theory of atoms-in-molecules, the potential function is the electron charge density distribution $\rho(r)$, and except for topical examples, the basins are located around the nuclei (atomic basins).

Another potential function closely related to Pauli principle is the electron localization function (ELF), denoted $\eta(r)$. The ELF function can be defined as

$$\eta(r) = \frac{1}{1 + \left(\frac{D^\sigma(r)}{D_o^\sigma(r)}\right)^2} \tag{1}$$

where $D^\sigma(r)$ stands for the excess local kinetic energy due to the Pauli repulsion. If the wave function is written as a single determinant, $D^\sigma(r)$ is expressed in terms of orbital contributions:

$$D^\sigma(r) = \frac{1}{2}\sum_i |\nabla\phi_i(r)|^2 - \frac{1}{8}\frac{|\nabla\rho(r)|^2}{\rho(r)} \tag{2}$$

and $D_o^\sigma(r)$ is the kinetic energy of the electron gas having the same density:

$$D_o^\sigma = C_F\rho(r)^{(5/3)} \tag{3}$$

where C_F is the Fermi constant. This function corresponds to an electronic localization index, varying between 0 and 1 (perfect localization). The reference value of 0.5 corresponds to a perfect delocalization (homogeneous electron gas). As a matter of fact, in the region of space where the Pauli repulsion is weak, the ELF value is close to unity, whereas in the opposite case, the ELF function tends to zero.

Since the ELF is a scalar function, the analysis of its gradient field allows to locate local maxima (attractors) and the corresponding basins. The partitioning thus obtained is consistent with the Lewis valence theory[15,16] and the VSEPR model of Gillespie.[17] Each of these attractors (and their corresponding basins) have a precise chemical meaning, due to the physical definition of ELF. There are two chemical types of basins: the core basins labeled *C*(atom symbol) and the valence basins, *V*(list of atoms). The structure provided by the core basins closely matches the inner atomic shell structure.[18] With the aim of differentiating the valence basins, the synaptic order has been defined by taking into account the boundaries between valence and core basins.[19] Monosynaptic basins correspond to lone pairs in the Lewis theory, disynaptic ones to two center bonds, and higher polysynaptic basins to multicentric bonds. Graphical representations of the bonding are obtained by plotting isosurfaces of the ELF function which define the volumes where the Pauli repulsion is rather weak. The localization domains, thus defined, are called reducible when they contain more than one attractor and called irreducible otherwise.

Having a well-defined mathematical partitioning of the space, it is possible to integrate the electronic density $\rho(r)$, over the Ω_i basin, to calculate basin populations:[18−21]

$$\bar{N}(\Omega_i) = \int_{\Omega_i}\rho(r)\,\mathrm{d}r \tag{4}$$

A combination of ELF and AIM analysis allows the definition of atomic sub-basins as the intersections of localization basins with atomic basins. The contribution of atom A to the Ω_i basin population is the integral of the electron density over the sub basin $\Omega_i \cap \Omega_A$ and can be calculated as follows:[22]

$$\bar{N}(\Omega_i)|A = \int_{\Omega_i\cap\Omega_A}\rho(r)\,\mathrm{d}r \tag{5}$$

The variance of the basin population is defined by[23,24]

$$\sigma^2(\bar{N};\Omega_i) = \langle N^2\rangle_{\Omega_i} - \langle N\rangle_{\Omega_i}^2 \tag{6}$$

and it can be readily written in terms of contributions arising from the other basins (covariance, B_{ij}) according to[25]

$$\sigma^2(\bar{N};\Omega_i) = \sum_{j\neq i}\bar{N}(\Omega_i)\bar{N}(\Omega_j) - \bar{N}(\Omega_i,\Omega_j) = \sum_{j\neq i}B_{ij} \tag{7}$$

In this expression, $\bar{N}(\Omega_i)\bar{N}(\Omega_j)$is the number of electron pairs classically expected from the basin population, whereas $\bar{N}(\Omega_i,\Omega_j)$- is the actual number of pairs obtained by integration of the pair

function over the basins Ω_i and Ω_j. The variance, $\sigma^2(\bar{N}_i,\Omega_i)$, is a measure of the quantum mechanical uncertainty of the basin population, which can be interpreted as a consequence of the electron delocalization, whereas the pair covariance, B_{ij}, indicates how much the population fluctuations of two given basins are correlated. The quantities B_{ij} calculated with the AIM partitioning are usually indicated by $\lambda_c(\rho)$ and have been defined as one-half of the topological bond order, TBO $= 2*\lambda_c(\rho)$, by Ángyan et al.[26] This definition is based on the partitioning of the exchange contribution to the second order density matrix independently of any variance calculation. Fradera et al. propose to substitute the term TBO by "delocalization index" because these quantities provide a natural picture of electron delocalization.[27]

Finally, it is useful to introduce the relative fluctuation of the basin populations within the Ω_i basin:

$$\lambda(\bar{N}_i;\Omega_i) = \frac{\sigma^2(\bar{N};\Omega_i)}{\bar{N}(\Omega_i)} \tag{8}$$

which is positive and expected to be less than 1 in most cases. Generally, a relative fluctuation larger than 0.45 indicates delocalization.[19]

3. Computational Method

Calculations were performed with the Gaussian 98 program,[28] using the hybrid Hartree−Fock density functional B3LYP[29,30] method. It has been recently proved that accurate values of structural properties can be obtained with this method for second-row transition metal dinuclear complexes.[4−6]

The B3LYP scheme used in conjunction with four basis sets gives a self-consistent set of results. The first two consist of the standard 3-21G and the 3-21G** basis sets for all atoms. In addition to the all-electron (AE) calculations, we have also used two effective core potentials (ECP): the standard CEP-121G triple-split basis[31] and the double-ζ pseudo-orbital basis set LanL2DZ, in which the metal atoms are represented by the relativistic effective core LANL2 potential (RECP) of Los Alamos.[32]

The ELF calculations were carried out with the TopMod package developed at the Laboratoire de Chimie Théorique de l'Université Pierre et Marie Curie.[33,34] Isosurfaces have been visualized with the public domain scientific visualization and animation program for high performance graphic workstations named SciAn.[35]

4. Results and Discussion

4.1. Chemical Bond in $Mo_2(HNCHNH)_4$. *4.1.1. Geometry Optimization.* The $Mo_2(HNCHNH)_4$ dimer belongs to the M_2L_4 tetrabridged compounds with a "paddlewheel" type structure, one of the most commonly structural types in dinuclear compounds containing metal−metal bonds. This compound has been taken as a model for the crystallographically characterized $Mo_2(RNCHNR)_4$ (R = *p*-$CH_3C_6H_4$).[36] Previous DFT geometry optimizations on $Mo_2(HNCHNH)_4$ carried out in a D_4 symmetry have shown that this model compound prefers an eclipsed configuration with a dihedral N−Mo−Mo−N angle close to zero (experimental value is 3.2°) for $Mo_2(RNCHNR)_4$); as a consequence, our calculations were carried out in a D_{4h} symmetry with the dihedral N−Mo−Mo−N angle fixed to zero.[4] In this study, Cotton et al. report the excellent performance in the geometry optimization of these systems for the combination B3LYP method and 3-21G basis sets, and they point out that less computer demanding satisfactory results could be obtained incorporating an ECP approximation into the DFT calculation. In this work, we have investigated the effect of adding polarization functions to the 3-21G basis sets for the nonmetal atoms (3-21G**) and the use the CEP-121G pseudopotential. The optimized geometry parameters for $Mo_2(HNCHNH)_4$ are listed in Table 1.

TABLE 1: Optimized and Experimental Structural Parameters (distances in Å and Angles in Degrees) for the Mo_2(formamidinate)$_4$ Model Dimer[a]

	3-21G	3-21G**	LanL2DZ	CEP-121G	exptl[b]
Mo−Mo	2.093	2.092	2.141	2.148	2.085
Mo−N	2.157	2.159	2.151	2.157	2.17
N−C	1.335	1.337	1.344	1.352	1.30
MoMoN	92.81	92.85	92.32	92.40	92.3
MoNC	117.53	117.51	118.89	118.16	117.0
NCN	119.30	119.26	118.89	118.89	121.0
NMoMoN	0.0 (fixed)	0.0 (fixed)	0.0 (fixed)	0.0 (fixed)	3.2

[a] All calculations were performed with the B3LYP functional at the level shown. [b] Average bond distances and angles from crystal structure data of $Mo_2(RNCHNR)_4$ (R = p-CH_3C6H4). See ref 36.

Addition of polarization functions to the 3-21G basis set results in optimized structural parameters closer to the experimental values, while the use of the CEP-121G pseudopotential does not present any clear advantages versus the LANL2 effective core potential of Los Alamos.

4.1.2. AIM and ELF Analyses on the Mo−Mo Bond. The difficulties in the interpretation of "closed-shell" (ρ_c high and $\nabla^2\rho_c < 0$) versus "open-shell" (ρ_c low and $\nabla^2\rho_c > 0$) chemical interactions raised when topological AIM criteria associated with the electron density and its laplacian are used have been already pointed out in the Introduction. In an attempt to improve the classification of chemical interactions, Bianchi et al. have introduced some energetic criteria based on the previously mentioned ideas of Cremer and Kraka.[9,13] These authors have demonstrated that the sign of the total energy, $E(r_c)$, where $E(r_c)$ is the sum of the kinetic, $G(r_c)$, and the potential $V(r_c)$ energy densities, is an index of the amount of covalency in a chemical interaction. A covalent bond has $V(r_c) \ll 0$, $G(r_c) \ll |V(r_c)|$, and $E(r_c) \ll 0$. Bianchi's energetic criteria makes the distinction between "dative bond" ($V(r_c) < 0$, $G(r_c) \cong |V(r_c)|$, and $E(r_c) < 0$) and "metallic bond" ($V(r_c) < 0$, $G(r_c) \cong |V(r_c)|$, and $E(r_c) < 0$ with $|E(r_c)| \cong 0$) as specific cases of the closed-shell interaction.

Although most of these criteria often yield results in agreement with the chemical common sense, it must be recalled that there is not obvious chemical reason to justify the way they were chosen. Indeed, Bianchi et al. concluded their paper on the chemical bond in $Mn_2(CO)_{10}$[9] with the statement "the proposed classification of the bonding interactions needs confirmation by further topological studies". Our results on the AIM topological properties of the Mo−Mo, Mo−N, and N−C bonds at the bond critical point (r_c) in the $Mo_2(HNCHNH)_4$ model dimer are summarized in Table 2.

Using the bond critical point criteria, the N−C bond can be unambiguously characterized as covalent since both $\nabla^2\rho(r_c)$ and $E(r_c)$ are negative, independent of the level of the calculation. The Mo−N and Mo−Mo bonds are more puzzling. The criteria of Bianchi et al. consider the Mo−N interaction as an intermediate case between "metallic" and "dative" bond since $E(r_c)$ is always negative and small whereas the Mo−Mo bond appears to be drifted toward the "dative" side. This is a rather uncomfortable situation because it contradicts indisputable symmetry and electronegativity arguments.

TABLE 2: Bond Critical Point Data for the Mo_2(Formamidinate)$_4$ Dimer

bond	basis	$\rho(r_c)$ (e Å^{-3})	$\nabla^2\rho(r_c)$ (e Å^{-5})	$G(r_c)$ (hartree Å^{-3})	$V(r_c)$ (hartree Å^{-3})	$E(r_c)$ (hartree Å^{-3})
Mo−Mo	3-21G**	0.185	0.550	0.250	−0.363	−0.113
	3-21G	0.185	0.549	0.250	−0.362	−0.112
	lanL2DZ	0.166	0.518	0.203	−0.276	−0.073
	CEP-121G	0.165	0.420	0.193	−0.282	−0.089
Mo−N	3-21G**	0.084	0.359	0.099	−0.109	−0.010
	3-21G	0.084	0.362	0.100	−0.110	−0.010
	lanL2DZ	0.086	0.365	0.104	−0.117	−0.013
	CEP-121G	0.085	0.333	0.100	−0.116	−0.016
N−C	3-21G**	0.313	−0.674	0.180	−0.528	−0.348
	3-21G	0.314	−0.668	0.184	−0.536	−0.352
	lanL2DZ	0.312	−0.710	0.188	−0.554	−0.366
	CEP-121G	0.300	−0.880	0.187	−0.594	−0.407

[a] All calculations were performed with the B3LYP functional at the level shown.

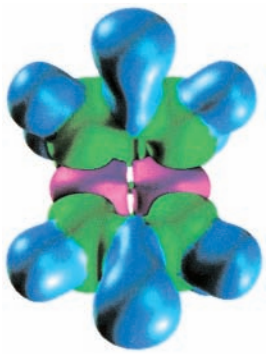

Figure 2. ELF isosurfaces (0.37) for $Mo_2(HNCHNH)_4$.

The calculated atomic basin populations for Mo, C, and N are 40.89, 5.21, and 8.03 e$^-$, respectively. The hydrogen atomic basin populations are less than one electron, namely, 0.84 e$^-$ for the H atom linked to the C atom and 0.63 e$^-$ for the H atom linked to the N atom. The net charge transfer from each formamidinato ligand to the two metal ions, formally considered as Mo^{2+}, is small, 0.44 e$^-$. The Mo−Mo delocalization index has a rather large value compared to the Mo−N one: 1.525 versus 0.296. On the other hand, the N−N index of 0.113 indicates the delocalization of the C−N bonds within the complex. The populations calculated through the AIM analysis allows us to identify the Mo−N interaction as dative, whereas the Mo−Mo interaction requires further analysis for an unambiguous characterization.

4.1.3. ELF Analysis. The ELF isosurface with $\eta(r) = 0.37$ for $Mo_2(HNCHNH)_4$ is displayed in Figure 2. At this level, seven reducible domains can be identified: four correspond to the ligand valence shell (in green) that include the *V*(Mo−N), *V*(C−N), *V*(C−H), and *V*(N−H) attractors, two to the molybdenum cores (in magenta), and the tiny green one to the *V*(Mo,-Mo) attactors. This latter domain contains four equivalent attractors lying in the σ_h plane. The valence basin populations computed with different basis sets at the all electron and effective core pseudopotential level are given in Table 3.

The electron population values calculated with the 3-21G and 3-21G** basis sets are very similar, whereas the pseudopotential calculations gives higher *V*(C,H) and *V*(Mo,Mo) populations. The Mo−Mo bond can be considered as quadruple, taking into account the four *V*(Mo,Mo) basins as previously pointed out by Nesper and Savin for the $[Mo_2Cl_8]^{4-}$ quadruply bonded dimer,[8] although the sum of the *V*(Mo,Mo) populations is only 0.6 e$^-$. Indeed, as in the case of the true metallic bond, the number of attractors between two metal atom cores (as well as their populations) is mainly driven by the symmetry and by the Pauli repulsion exerted by these cores.[37] Stronger Pauli repulsion results in smaller ELF values for the *V*(Mo,Mo) attractor and lower basin populations. Upon an increase of the Mo−Mo distance, the ELF value at the *V*(Mo,Mo) attractor and its basin population increases, as can be seen when comparing the AE ($R \cong 2.092$ Å) and pseudopotential ($R \cong 2.148$ Å) results.

TABLE 3: Valence Population (e$^-$) for the Mo_2(Formamidinate)$_4$ Dimer[a]

basin	3-21G**	3-21G	LanL2DZ	CEP-121G
V(C,H)	2.17	2.25	2.46	2.59
V(N,H)	1.85	1.74	1.85	1.77
V(C,N)	2.03	1.99	2.04	2.04
V(N,Mo)	3.88	3.78	3.62	3.76
V(Mo,Mo)	4 × 0.15	4 × 0.12	4 × 0.35	4 × 0.40

[a] All calculations were performed with the B3LYP functional at the level shown.

TABLE 4: Atomic Basin Contribution for the Mo_2(Formamidinate)$_4$ Model Dimer (B3LYP/3-21G)**

basin	$\bar{N}$	Mo	N	C	H
V(C,H)	2.17	−	−	1.23	0.94
V(N,H)	1.87	−	1.22	−	0.65
V(C,N)	2.03	−	1.11	0.92	−
V(N,Mo)	3.88	0.12	3.76	−	−
V(Mo,Mo)	4 × 0.15	4 × 0.075	−	−	−

To distinguish and to quantify the close-shell versus shared interaction, the atomic basin (AIM) contribution to the disynaptic basins has been calculated at the 3-21G** AE level, and the results are listed in Table 4.

The *V*(C,H), *V*(N,H), and *V*(C,N) basins correspond to covalent (shared) interactions because the atomic basin of the two linked atoms noticeable contribute to their population, the different contributions being due to electronegativity differences. The *V*(N,Mo) basin is essentially populated thanks to the nitrogen atomic basin density being clearly of the "donnor−acceptor" type. However, the classification of the Mo−Mo interaction is less straightforward partly due to the low *V*(Mo,-Mo) populations and because there is a huge electronic delocalization between the two metallic cores, testified by the C(Mo) covariance contribution to the C(Mo) variance. A summary of relevant topological data for all compounds investigated is presented in Table 5.

The origin of the low values for the *V*(Mo,Mo) population, compared to the expected one based on the "nominal bond order" value of four (8 e$^-$), is certainly the ambivalent character of the "d" orbitals that can be considered as core orbitals and as valence orbitals depending on the nature of the chemistry under study. In the case of solid metals, it has been found that the transition metal "d" orbitals almost do not contribute to the interstitial density.[37] In the present, case the orbital contributions to the *C*(Mo) and *V*(Mo,Mo) basin provide the pertinent information (see Table 5, second column): the molecular orbitals involving the "4d" function of the metal (denoted E_u, A_{1g} and B_{2g} in the dimer D_{4h} symmetry) essentially contribute to the *C*(Mo) populations.

The *V*(Mo,Mo) basins are not the dominant feature of the interaction due to their low population values. The covariance analysis of the *C*(Mo) basins provide a clue for understanding the singularities of these metal core basins. In general, the covariance term between two core basins is very low; for example, those related to the N and C cores are 0.002. The Mo−Mo core covariance has an abnormally high value, 1.255,

TABLE 5: Geometrical and Topological Data for M_2(formamidinate)$_4$ Complexes (B3LYP/3-21G)[a,b]**

	Nb	Mo	Tc	Ru	Rh	Pd
BO	3	4	3	2	1	0
d(M−M)$_{exp}$ (Å)		2.085		2.475	2.434	2.622
d(M−M)$_{cal}$ (Å)	2.224	2.092	2.082	2.493	2.459	2.691
$\rho(r_c)$ (e Å^{-3})	0.147	0.185	0.179	0.079	0.072	0.042
$\nabla^2\rho(r_c)$ (e Å^{-5})	0.392	0.550	0.609	0.168	0.158	0.115
$G(r_c)$ (hartree Å^{-3})	0.178	0.250	0.245	0.054	0.053	0.039
$V(r_c)$ (hartree Å^{-3})	−0.257	−0.363	−0.337	−0.067	−0.066	−0.050
$E(r_c)$ (hartree Å^{-3})	−0.079	−0.113	−0.092	−0.013	−0.013	−0.011
$\bar{N}$(M)	39.74	40.89	41.96	42.97	43.95	45.15
$\lambda_c(\rho)$	1.257	1.497	1.356	0.661	0.504	0.130
TBO = 2*$\lambda_c(\rho)$	2.514	2.994	2.712	1.321	1.008	0.260
C(C)	2.13	2.14	2.12	2.13	2.13	2.12
C(N)	2.12	2.12	2.11	2.09	2.15	2.12
C(M)	39.05	40.12	41.50	42.47	43.42	44.42
V(C,H)	2.18	2.18	2.24	2.19	2.16	2.20
V(N,H)	1.88	1.86	1.84	1.88	1.84	1.86
V(C,N)	2.03	2.01	1.94	2.00	1.99	1.92
V(M,N)	3.68	3.72	3.78	3.70	3.69	3.79
V(M.M)	0.17 × 4	0.15 × 4	−	0.25	0.32	−
V(M,N)| M	0.10	0.12	0.12	0.10	0.10	0.04
V(C,N)| N	0.89	0.88	1.05	1.12	1.04	1.01
C(M))| E_u	0.81	0.81	0.79	0.87	0.78	- -
C(M))| A_{1g}	0.80	0.82	0.79	0.85	0.62	- -
C(M))| B_{2g}	- -	0.64	0.76	0.69	- -	- -
V(M,M))| E_u	0.05	0.04	- -	- -	0.05	- -
V(M,M))| A_{1g}	0.07	0.04	- -	0.14	0.19	- -
V(M,M))| B_{2g}	- -	0.01	- -	- -	- -	- -
B(M,M)	1.025	1.255	1.371	0.551	0.373	0.124

[a] Atomic and basin populations are given in electrons. [b] Experimental M−M bond distances are taken from crystal structure data of M_2(RNCHNR)$_4$ (R = p-CH_3C6H4). See ref 4 and references therein.

which represents about 80% of the covariance of the Mo atomic basins. Ángyán et al. have identified the atomic basins covariances, $\lambda_c(\rho)$, as half the bond order by generalizing Mayer's definition.[26] In the case of $Mo_2(HNCHNH)_4$, the Mo−Mo bond order calculated with the formula of Ángyán is 2.994, a value close to the MO expectation.

The large electron fluctuation which occurs between the two metallic cores can be interpreted in terms of simple resonance arguments. Because the metal dimer is in a closed-shell singlet state, there is no spin polarization, and each metallic core should be considered as a local closed-shell subsystem whose orbitals fulfill the C_{4v} point group symmetry requirements. The Mo core population is close to 40 e^- with a covariance of 1.255, and as a consequence, an average of four out of the six electrons formally considered as valence according to the MO theory should now be incorporated into the core. Following the traditional greek characters usually used to described the quadruple metal−metal bonding MOs ($\sigma^2\pi^4\delta^2$), the following core configurations are compatible with the molecular symmetry: [Kr]π^4, [Kr]$\sigma^2\delta^2$, and [Kr]$\pi^4\delta^2$ and [Kr]σ^2, [Kr] $\pi^4\sigma^2$, and [Kr]δ^2. A resonance structure between the first two configurations, Mo([Kr]π^4)−Mo([Kr]$\sigma^2\delta^2$) ↔ Mo([Kr]$\sigma^2\delta^2$)−Mo([Kr]π^4), corresponds to an average core population of 40 e^- with a variance of zero.

To recover the calculated covariance between the Mo atoms of 1.255, resonant structures that involve the remaining configurations must be considered. The resonant structures Mo([Kr]$\pi^4\delta^2$)−Mo([Kr]σ^2) ↔ Mo([Kr]σ^2)−Mo([Kr]$\pi^4\delta^2$) and Mo([Kr] $\pi^4\sigma^2$)−Mo([Kr] δ^2) ↔ Mo([Kr]δ^2)−Mo([Kr]$\pi^4\sigma^2$) have an average population of 40 core electrons, with an standard deviation (σ) of 2 and consequently a variance (σ^2) of 4. The calculated covariance of 1.255 can be approximately recovered, assuming that these two last resonant structures contribute altogether with a $^1/_4$ weight factor while the first resonant structure, namely, that Mo([Kr]π^4)−Mo([Kr]$\sigma^2\delta^2$) ↔ Mo([Kr]$\sigma^2\delta^2$)−Mo([Kr]π^4) contributes with a weight factor of $^3/_4$. The orbital ordering energies—$E_u{}^4A_{1g}{}^2$, and ligand-based orbitals, $B_{2g}{}^2$ (or $\pi^4\sigma^2...\delta^2$), with the π and σ orbital very close in energy—are consistent with the observed photoelectronic spectrum, and this energy ordering supports the higher weight assigned to the resonance structure that incorporates the low lying E_u(or π) metal "d" orbitals into the core. In addition, the "d" orbitals are the main contributors to the population of the four V(Mo,Mo) basins (53% π, 27% σ, and 7% δ).

The metal "d" orbitals are the responsible of the Mo−Mo interaction, in the first place through its involvements in the delocalization of the electron density between the molybdenum cores and in the second place through its contribution to the intermetallic disynaptic basin. In our opinion, the crucial factor of the metal−metal bond is the first aspect, and as a matter of fact, such a fluctuation evaluated through the delocalization index has been referred to as topological bond order. This topological analysis of the quadruple M−M bond gives an alternative interpretation to the one provided by the MO theory. The overlap between metal "d" orbitals responsible of the metal−metal bond in the MO theory has been substituted in the ELF topological description by the concepts of delocalization of the core electrons and the formation of disynaptic intermetallic basins. While this last aspect has been related to the concentration of electron density due to orbital overlaps, the concept of electron density delocalization between atomic basins has no analogue in the MO theory.

4.2. Chemical Bond in $M_2(HNCHNH)_4$ (M = Nb, Mo, Tc, Ru, Rh, and Pd). The optimized geometry parameters for these formamidinate dimers are summarized in Table 5, together with the topological analysis results. The AIM analysis enables a classification of these complexes in two groups; the first one that includes Nb, Mo, and Tc has shorter metal−metal bond distances (between 2.08 and 2.22 Å), $\rho(r_c)$ values of ca. 0.15 e^-/Å^3, and a total energy density, $E(r_c)$, of ca. −0.1 hartree/Å^3.

TABLE 6: Resonant Structures, Estimated and Calculated Core Populations, *C*(*M*), and Covariances, *B*(*M*,*M*), in E$^-$, for the Metal−Metal Bond in M_2(formamidinate)$_4$ Dimers

M	resonant structures, (weight)	standard deviation (σ)	covariance (σ^2)	C_{est}(M)	B_{est}(M,M)	C_{calc}(M)	B_{cal}(M,M)
Nb	M([Kr]π^4)−M([Kr]σ^2) ↔ M([Kr]σ^2)− M([Kr]π^4), (1)	1	1	39	1	39.05	1.025
Mo	M([Kr]π^4)−M([Kr]$\sigma^2\delta^2$) ↔ M([Kr]$\sigma^2\delta^2$)−M([Kr]π^4), (3/4)	0	0	40	1	40.12	1.255
	M([Kr]$\pi^4\delta^2$)−M([Kr]σ^2) ↔ M([Kr]σ^2)−M([Kr]π^4 δ^2), (1/8)	2	4				
	M([Kr]$\pi^4\sigma^2$)−M([Kr]δ^2) ↔ M([Kr]δ^2)−M([Kr]$\pi^4\sigma^2$), (1/8)	2	4				
Tc	M([Kr]$\pi^4\delta^2$)−M([Kr]$\sigma^2\delta^2$) ↔ M([Kr]$\sigma^2\delta^2$)−M([Kr]π^4 δ^2), (1)	1	1	41	1	41.50	1.371
Ru	M([Kr]$\pi^4\delta^2$)−M([Kr]$\pi^4\sigma^2$) ↔ M([Kr]$\pi^4\sigma^2$)−M([Kr]$\pi^4\delta^2$), (7/8)	0	0	42	0.5	42.47	0.551
	M([Kr]π^4)−M([Kr]$\pi^4\sigma^2\delta^2$) ↔ M([Kr]$\pi^4\sigma^2\delta^2$)−M([Kr]π^4), (1/8)	2	4				
Rh	M([Kr]π^4)−M([Kr]$\pi^4\sigma^2\delta^2$) ↔ M([Kr]$\pi^4\sigma^2\delta^2$)−M([Kr]π^4), (1/8)	2	4	43.75	0.25	43.42	0.373
	M([Kr]$\pi^4\sigma^2\delta^2$)−M([Kr]$\pi^4\sigma^2\delta^2$), (7/8)	0	0				
Pd	M([Kr]$\pi^4\sigma^2\delta^2$)−M([Kr]$\pi^4\sigma^2\delta^2$)	0	0	44	0	44.52	0.116

The second group with longer M−M bond distances (between 2.45 and 2.69 Å) has $\rho(r_c)$ and $E(r_c)$ values close to zero. As previously mentioned for the Mo dimer, the metal−metal bond can be classified as a closed-shell interaction of the "dative" type for the first group and as a metallic interaction for the second group. The ambiguity in classifying the metal−metal bond using only these AIM criteria is again evident.

The net ligand to metal charge transfer in the series are 0.37, 0.44, 0.48, 0.48, 0.55, and 0.58 e$^-$ for Nb, Mo, Tc, Ru, Rh, and Pd, respectively. This fact explains the small variation observed for the valence basin population of the ligand with the nature of the metal.

The ELF topological analysis shows no disynaptic *V*(M,M) basins for the dimers with the shortest and the longest intermetallic distance, Tc and Pd, respectively, and there is a single basin for Ru and Rh and four for Nb and Mo. The sums of the *V*(M,M) basin populations, if any, are very similar: 0.68, 0.60, 0.25, and 0.32 e$^-$ for Nb, Mo, Ru, and Rh, respectively. The attractor multiplicity depends on the metal−metal distance and seems to be a consequence of the Pauli repulsion between the metallic cores. The only attractor found for the Ru and Rh system is split into four components as the M−M distance decreases (Nb and Mo), and they disappear at shorter intermetallic distances (Tc). In addition, the ELF value at the bond midpoint decreases as the bond length increases, and there is no attractor for the Pd derivative.

As observed for the molybdenum system, the core−core covariance accounts for approximately 80% of the metal−metal covariance in all complexes. The value of the core−core delocalization indexes can also be rationalized by simple resonance concepts. The proposed resonance structures for each metal dimer, together with their weight factors and the estimated covariances, are compared in Table 6 with the calculated populations of the core metal basins, *C*(M), and their covariance values, *B*(M,M).

In the cases of Nb_2(formamidinate)$_4$ ($\sigma^2\pi^4$) and Tc_2-(formamidinate)$_4$ ($\sigma^2\pi^4\delta^2\delta^{*2}$), with an odd number of electrons per metal atoms, the only resonance structures compatible by symmetry are the ones listed in Table 6, and the estimated *B*(M,M) covariances of 1 are close to the calculated values. The population and covariances estimated for the Ru core basin in Ru_2(formamidinate)$_4$ can be understood assuming two different resonance structures for this dimer as listed in Table 6. These resonance structures must be compatible with the "metal-based" orbital energy ordering of ($\sigma < \pi < \delta < \pi^*$). As in the molybdenum system, different weight factors have been assigned to these structures in order to reproduce the calculated *C*(M) and *B*(M,M) values. The Pd dimer presents a unique possibility for the core configuration, namely, M([Kr]$\pi^4\sigma^2\delta^2$)−M([Kr]$\pi^4\sigma^2\delta^2$), and consequently the covariance between the core populations must be zero, a value close to the calculated value of 0.116.

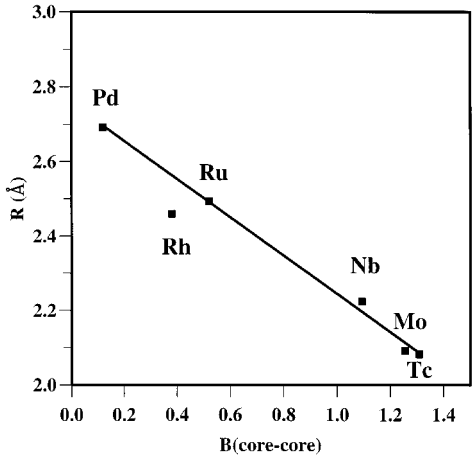

Figure 3. Metal−metal bond distances vs the core covariance, *B*(*M*,*M*) for M_2(HNCHNH)$_4$.

The Rh case is more puzzling because the expected behavior based on extrapolating the previous results, that is, a resonance structure of the form M([Kr]π^4 δ^2)−M([Kr]$\pi^4\delta^2\sigma^2$) ↔ M([Kr] π^4 $\delta^2\sigma^2$)−M([Kr]$\pi^4\delta^2$) with a covariance of 1, does not reproduce the observed *B*(M,M) values of 0.373. The rhodium complex is an exception in the series because the idealized D_{4h} symmetry is far from the energy minimum (the optimized N−Rh−Rh−N dihedral angle is 13°**),** causing a strong interaction between the metal "d" orbitals and the ligand. The optimized geometry of the rhodium dimer is in good agreement with the experimental one; in particular, the observed distortion from D_{4h} to D_4 is well accurately accounted for. On the basis of the core basin populations and their covariances, one is tempted to consider the configuration of the rhodium metal as an intermediate case between the above resonant structure and the one of Pd, namely, M([Kr]π^4 $\sigma^2\delta^2$)−M([Kr]$\pi^4\sigma^2\delta^2$), with variances of four and zero, respectively. If we assume a weight factor of $^1/_8$ for the first resonant structure, we obtain an estimated covariance of 0.25 close to the calculated values of 0.373, although in this case, the estimated core population is higher than the observed one.

Except for Rh, there is an excellent correlation between the core covariances, *B*(M,M) and the metal−metal distances, as seen in Figure 3. This result confirms our assumption about the higher significance of the delocalization of the electron density between the metallic cores versus the formation of a disynaptic intermetallic basin.

This correlation applies also for Tc_2(formamidinate)$_4$, for which the shortest intermetallic distance has been calculated in apparent contradiction with a lower MO bond order (three) as compared with that of the molybdenum dimer with a quadruple

metal bond. It is important to point out that no intermetallic basin has been observed for this technecium dimer. On the other hand, the apparent contradiction between the experimental and calculated bond distances for Ru and Rh with the MO bond orders cannot be overcome with these topological analysis, although as already mentioned, the rhodium dimer constitutes an exception within the series.

5. Concluding Remarks

In this paper, we have attempted to describe, characterize, and rationalize the nature of the metal−metal bond encountered in the M_2L_4 (M = Nb, Mo, Tc, Ru, Rh, and Pd) complexes with the help of topological arguments. Though the method of calculation is quite simple (limited basis sets, neglect of spin−orbit and relativistic effects), the overall agreement between the optimized geometries and the expected experimental values indicates the reliability of at least a qualitative interpretation.

The topological analysis of the electron localization function provides an alternative interpretation of the bonding relying on a local description. In the standard MO picture, the bonding between the metal centers results from the balance of the occupation of the A_{1g}, E_u, and B_{2g} canonical bonding orbitals, also named σ, π, and δ, respectively, involving mainly the metal 4d AOs with their antibonding counterparts (A_{2u}, E_g, and B_{1u}). This picture yields bond orders ranging from 0 to 4 which correlate well with the M−M distances, except for the apparent contradiction found in the Tc and Mo dimers and in Rh and Ru complexes.

The basic assumption of the MO picture is that the 4d orbitals of transition metals are valence orbitals and should be treated accordingly. However, their energies and their exponents are closer to those of the 4d orbitals at the right side main group elements of the same row, i.e., Ag (which are always considered as core orbitals), than to those of standard ns and np valence orbitals. In fact the MO picture is biased by the ambivalence of these 4d AOs, and as a consequence, the use of derived concepts as bond orders require an extreme care.

The picture of the bonding emerging from the topological analysis is that of a strong resonance interaction due to the fluctuation of the number of electrons within the core areas. The magnitude of the fluctuation is given by the core delocalization indexes which are almost linearly correlated with the M−M distances.

Acknowledgment. Financial support from Ministerio de Educación y Ciencia (DGESIC, Research Project PB98-1044) and Fundació Caixa Castelló-UJI (Research Project P1B98-07) is gratefully acknowledged. B.S. thanks the Iberdrola Foundation for financing his stay as a visiting professor at the Universitat Jaume I.

References and Notes

(1) Cotton, F. A. *Multiple Bonds Between Metal Atoms*, 2nd ed.; Oxford University Press: Oxford, 1993.
(2) Cotton, F. A. *Inorg. Chem.* **1998**, *37*, 5710.
(3) Cotton, F. A. *Inorg. Chem.* **1965**, *4*, 334.
(4) Cotton, F. A.; Feng, X. *J. Am. Chem. Soc.* **1997**, *119*, 7514.
(5) Cotton, F. A.; Feng, X. *J. Am. Chem. Soc.* **1998**, *120*, 3387.
(6) Demachy, I.; Lledos, A.; Jean, Y. *Inorg. Chem.* **1999**, *38*, 5443.
(7) Lichtenberger, D. L.; Lynn, M. A.; Chisholm, M. H. *J. Am. Chem. Soc.* **1999**, *121*, 12167.
(8) Savin, A.; Nesper, R.; Wengert, S.; Fässler, T. *Angew. Chem., Int. Ed. Engl.* **1997**, *36*, 1808.
(9) Bianchi, R.; Gervasio, G.; Marabello, D. *Inorg. Chem.* **2000**, *39*, 2360.
(10) Bader, R. F. W. *Atoms in Molecules: A Quantum Theory*; Oxford University Press: Oxford, 1990.
(11) Macchi, P.; Proserpio, D. M.; Sironi, A. *J. Am. Chem. Soc.* **1998**, *120*, 13429.
(12) Bianchi, R.; Gervasio, G.; Marabello, D. *Chem. Commun.* **1998**, 1535.
(13) Cremer, D.; Kraka, E. *Angew. Chem., Int. Ed. Engl.* **1984**, *23*, 67.
(14) Llusar, R.; Beltrán, A.; Andrés, J.; Noury, S.; Silvi, S. *J. Comput. Chem.* **1999**, *20*, 1517.
(15) Lewis, G. N. *J. Am. Chem. Soc.* **1919**, *38*, 762.
(16) Lewis, G. N. *Valence and the Structure of Atoms and Molecules*; Dover: New York, 1966.
(17) Gillespie, R. J. *Molecular Geometry*; Van Nostrang Reinhold: London, 1972.
(18) Kohout, M.; Savin, A. *Int. J. Quantum Chem.* **1996**, *60*, 875.
(19) Savin, A.; Silvi, B.; Colonna, F. *Can. J. Chem.* **1996**, *74*, 1088.
(20) Häussermann, U.; Wengert, S.; Hofmann, P.; Savin, A.; Jepsen, O.; Nesper, R. *Angew. Chem., Int. Ed. Engl.* **1994**, *33*, 2069.
(21) Häussermann, U.; Wengert, S.; Nesper, R. *Angew. Chem., Int. Ed. Engl.* **1994**, *33*, 2073.
(22) Jansen, G. *International Conference on Chemical Bonding: State of the Art in Conceptual Quantum Chemistry*; La Colle-sur-Loup, France, 2000; p 42.
(23) Messiah, A. *Mécanique Quantique*; Dunod: Paris, 1962.
(24) Diner, S.; Claverie, P. In *Statiscal and Stochastic Aspects of the Delocalization Problem in Quantum Mechanics*; Cjhalvet, O., Daudel, R., Diner S., Malrieu, J. P., Eds.; Reidel: Dordrecht, 1976; Vol. II, p 365.
(25) Noury, S.; Colonna, F.; Savin, A.; Silvi, B. *J. Mol. Struct.* **1998**, *450*, 59.
(26) Ángyán, J. G.; Loos, M.; Mayer, I. *J. Phys. Chem.* **1994**, *98*, 5244.
(27) Fradera, X.; Austen, M. A.; Bader, R. F. W. *J. Phys. Chem. A* **1998**, *103*, 304.
(28) Frisch, M. J.; Trucks, G. W.; Schlegel, H. B.; Scuseria, G. E.; Robb, M. A.; Cheeseman, J. R.; Zakrzewski, V. G.; Montgomery, J. A., Jr.; Stratmann, R. E.; Burant, J. C.; Dapprich, S.; Millam, J. M.; Daniels, A. D.; Kudin, K. N.; Strain, M. C.; Farkas, O.; Tomasi, J.; Barone, V.; Cossi, M.; Cammi, R.; Mennucci, B.; Pomelli, C.; Adamo, C.; Clifford, S.; Ochterski, J.; Petersson, G. A.; Ayala, P. Y.; Cui, Q.; Morokuma, K.; Malick, D. K.; Rabuck, A. D.; Raghavachari, K.; Foresman, J. B.; Cioslowski, J.; Ortiz, J. V.; Baboul, A. G.; Stefanov, B. B.; Liu, G.; Liashenko, A.; Piskorz, P.; Komaromi, I.; Gomperts, R.; Martin, R. L.; Fox, D. J.; Keith, T.; Al-Laham, M. A.; Peng, C. Y.; Nanayakkara, A.; Gonzalez, C.; Challacombe, M.; Gill, P. M. W.; Johnson, B.; Chen, W.; Wong, M. W.; Andres, J. L.; Gonzalez, C.; Head-Gordon, M.; Replogle, E. S.; Pople, J. A. *Gaussian 98*, Revision A.7 ed.; Gaussian, Inc.: Pittsburgh, PA, 1998.
(29) Becke, A. D. *J. Chem. Phys.* **1993**, *98*, 5648.
(30) Lee, C.; Yang, Y.; Parr, R. G. *Phys. Rev. B* **1988**, *37*, 785.
(31) Stevens, W. J.;.Krauss, M.; Bash, H.; Jasien, P. G. *Can. J. Chem.* **1992**, *70*, 612.
(32) Hay, P. J.; Wadt, R. *J. Chem. Phys.* **1985**, *82*, 299.
(33) Noury, S.; Krokidis, X.; Fuster, F.; Silvi, B. *TopMod Package*; Paris, 1997.
(34) Noury, S.; Krokidis, X.; Fuster, F.; Silvi, B. *Comput. Chem.* **1999**, *23*, 597.
(35) Pepke, E.; Murray, J.; Lyons, J.; T.-Z, H. *Scian (Supercomputer Computations Res. Inst.)*; Florida State University: Tallahassee, FL, 1993.
(36) Cotton, F. A. *Inorg. Chem.* **1989**, *28*, 594.
(37) Silvi, B.; Gatti, C. *J. Phys. Chem. A* **2000**, *104*, 947.